

Limestone Member of the Smithville Formation (upper Lower Ordovician) in northern Arkansas; and (v) the uppermost part of the Metaline Formation (Middle and ?Upper Cambrian) in north-eastern Washington (14). *Anatolepis heintzi* also occurs in upper Lower Ordovician strata of eastern Greenland (15, 16).

The report (17) of "Heterostracoderm fish" of Late Cambrian age from the Gros Ventre Formation of the Bighorn Mountains, Wyoming, must be considered as dubious until further study, including histologic sectioning, confirms the affinities of those objects. The published figures [plate 1, figures 1 and 2 in (17)] are inadequate for determination, and Denison (1, p. 134) notes that those fragments "have little resemblance to any known vertebrate."

The known occurrences of *Anatolepis* show that vertebrates were extant by the Late Cambrian and that these early fish were widely distributed by Early Ordovician time. These occurrences are restricted to tropical and subtropical localities around the Cambrian-Ordovician North American paleocontinent from approximately 20°N to 25°S (18). The presence of these fish in the stratigraphic units listed above, all of which are of undoubted marine origin, is also strong evidence for a marine habitat for the earliest vertebrates (1, 2, 19).

JOHN E. REPETSKI

U.S. Geological Survey, U.S. National Museum, Washington, D.C. 20560

#### References and Notes

1. R. H. Denison, *Fieldiana Geol.* **16**, 131 (1967).
2. K. A. Lehtola, *Contrib. Mus. Paleontol. Univ. Mich.* **24**, 23 (1973).
3. T. Bockelie and R. A. Fortey, *Nature (London)* **260**, 36 (1976).
4. T. Bockelie, D. L. Bruton, R. A. Fortey, *Nor. Polarinst. Arbok 1975* (1976), pp. 214-217.
5. A. Ritchie and J. Gilbert-Tomlinson, *Archeringa* **1**, 351 (1977).
6. The sample was collected by M. H. Staatz.
7. Trilobites identified from sample by M. E. Taylor include *Ellipsocephaloides* sp., *Ptychaspis striata* Whitfield, and ?*P. tuberosa* Feniak. These taxa indicate the *Ptychaspis-Prosaukia* Zone, Croixian Series, Franconian Stage.
8. Microprobe preparation and analysis were performed by E. Jarosewich and G. Moreland, whose help is appreciated.
9. R. H. Denison, *Fieldiana Geol.* **13**, 309 (1964).
10. *Anatolepis* sp. from high in the El Paso Group is shown as figure 4 in M. H. Nitecki, R. C. Gutschick, and J. E. Repetski [*Fieldiana Geol.* **35**, 1 (1975)].
11. Sample obtained from J. F. Miller.
12. R. H. Flower, *N.M. Bur. Mines Miner. Resour. Mem.* **12** (1964); the sample was collected by R. H. Flower.
13. The sample was obtained from R. L. Ethington.
14. The sample was collected by M. E. Taylor and E. Schuster from U.S. Geological Survey (USGS) fossil locality 8667-CO.
15. J. S. Peel (personal communication to E. L. Yochelson) and J. S. Peel and A. K. Higgins (personal communication) interpret *Anatolepis* as a merostome arthropod, based on its resemblance to merostomes portrayed by G. O. Raasch [*Geol. Soc. Am. Spec. Pap.* **19** (1939)]. The internal structure and composition of the Deadwood Formation specimens, however, argues for their assignment to the heterostracans.
16. A. R. Palmer recently informed me (personal

- communication) of the occurrence of *Anatolepis* in USGS fossil collections 2675-CO (Lincoln County, Nevada), 3503-CO (Bonneville County, Idaho), and 4352-CO (eastern Alaska). These collections are from Upper Cambrian strata.
17. N. E. Cygan and F. L. Koucky, *Wyo. Geol. Assoc. Billings Geol. Soc. 1st Joint Field Conf. Guideb.* (1963), pp. 26-37.
  18. A. G. Smith, J. C. Briden, G. E. Drewry, *Spec. Pap. Palaeontol. No. 12* (1973), pp. 1-42.
  19. R. H. Denison, *Fieldiana Geol.* **11**, 359 (1956).
  20. I thank the following for their help in preparation of various aspects of this report: F. C. Whit-

more, M. E. Taylor, and E. L. Yochelson critically read the manuscript; D. Dunkle, A. G. Harris, B. Runnegar, N. Hotton III, R. H. Denison, A. R. Palmer, and K. Towe contributed information, criticism, and advice; W. Ross, C. Smith, K. Moore, W. Pinckney, T. DeMoss, S. Braden, H. Mochizuki, and R. Johnson provided excellent technical assistance. After initial submission, this manuscript was improved thanks to critical reviews by Bobb Schaeffer and two anonymous reviewers.

16 September 1977; revised 19 January 1978

## The Structure of Crystalline Tris: A Plastic Crystal Precursor, Buffer, and Acetylcholine Attenuator

**Abstract.** *The crystal and molecular structure of the widely used buffer tris(hydroxymethyl)aminomethane (tris) has been determined from single-crystal diffractometer data to a standard agreement factor (R value) of 0.026 and bond length standard deviations of 0.002 angstrom. Tris crystallizes in the orthorhombic system, space group Pn2<sub>1</sub>a, with four molecules per unit cell; a = 8.844(1) angstroms, b = 7.794(1) angstroms, and c = 8.795(1) angstroms. The center-to-center distances of tris molecules in the ordered phase range from 0.4 to 1.0 angstrom less than they do in the orientationally disordered (plastic) phase of similar molecules.*

The compound tris(hydroxymethyl)aminomethane, H<sub>2</sub>NC(CH<sub>2</sub>OH)<sub>3</sub> (commonly known as tris or tham), is a widely used buffering agent (1) in the pH range 7 to 9, important for studies of physiological media and seawater (2). However, it was recently reported that tris antagonizes the action of ionophoretically applied acetylcholine on neurons of *Aplysia californica* (3). Wilson *et al.* suggested that the mechanism of

attenuation might be related to structural similarities between the acetylcholine and tris molecules.

Tris is also of interest for several other reasons. It has been proposed as a standard for solution calorimetry (4). The tris molecule is globular and forms an orientationally disordered (plastic) crystal at temperatures between 134°C and its melting point, 173°C (5), in a manner similar to the related polyhydric alcohol pentaerythritol [C(CH<sub>2</sub>OH)<sub>4</sub>] (6). Finally, good experimental values of hydrogen bonding in polyhydric molecules are needed in crystal packing computations used to determine the values of the parameters for the potential energy of the O-H<sub>4</sub> ··· O<sub>18</sub> hydrogen bond used in computations of the conformational energy of peptides (7).

In view of this current wide-ranging interest in tris, there is a need for a detailed characterization of the properties of this molecule. The results of a crystal structure analysis, presented here, will make it possible to carry out a structural comparison with acetylcholine, to furnish accurate hydrogen bond distances for use

Table 1. Intramolecular interatomic distances (angstroms).

Atoms	Distance (no riding correction)	Distance (riding correction)
A C(C)*-N	1.472(2)	1.479(2)
B C(C)-C(1)	1.522(2)	1.531(2)
C C(C)-C(2)	1.531(2)	1.538(2)
D C(C)-C(3)	1.522(2)	1.528(2)
Average C-C	1.525(2)	1.532(2)
E C(1)-O(1)	1.412(2)	1.435(2)
F C(2)-O(2)	1.426(3)	1.443(3)
G C(3)-O(3)	1.431(2)	1.438(2)
Average C-O	1.423(2)	1.436(2)
N-HN1	0.835(30)	
N-HN2	0.822(36)	
Average N-H	0.828	
C(1)-H11	0.928(31)	
C(1)-H12	0.959(32)	
C(2)-H21	0.998(30)	
C(2)-H22	0.964(35)	
C(3)-H31	1.031(27)	
C(3)-H32	0.966(30)	
Average C-H	0.974	
O(1)-HO1	0.739(49)	
O(2)-HO2	0.878(45)	
O(3)-HO3	0.984(42)	
Average O-H	0.867	

\*C(C) is the central carbon atom. Letter designations A through G identify intramolecular distances in Fig. 1.

Table 2. Average intramolecular angles.

Atom group	Angle (deg)
N-C(C)-C	108.7(0.2)
C-C(C)-C	110.3(0.2)
O-C-C(C)	110.3(0.2)
H-N-H	107.4(2.9)
H-N-C	108.4(2.2)
H-C-H	110.0(2.4)
H-C-O	109.8(1.8)
H-C-C(C)	108.5(1.8)
H-O-C	106.0(2.5)

Table 3. Hydrogen-bonded distances ( $D$ ),  $i-j\cdots k$ .

$i$	$j$	$k$	$D_{ik}$ (Å)	$D_{ij}$ (Å)	$D_{jk}$ (Å)	$\theta_{ijk}$ (deg)
O(3)	HO3	N	2.718(2)	0.984	1.737(40)	155.6
O(1)	HO1	O(2)	2.723(2)	0.739	2.021(50)	159.0
O(2)	HO2	O(3)	2.674(2)	0.878	1.797(45)	176.0
N	HN1	O(1)	3.051(3)	0.835	2.338(31)	143.7

in peptide and protein conformational analyses, and to describe the ordered form of a hydrogen-bonded plastic crystal precursor.

Tris crystallizes in the orthorhombic system, with  $a = 8.844(1)$  Å,  $b = 7.794(1)$  Å, and  $c = 8.795(1)$  Å. The experimental and x-ray densities are 1.320 and 1.327 g/ml, respectively, corresponding to four molecules per unit cell. The observed systematic absences are consistent with space group  $Pn2_1a$  (space group 33, nonstandard setting), which was confirmed during the refinement of the structure. We analyzed the data, collected on an automatic single-crystal diffractometer, using standard crystallographic programs. The resulting model (including both hydrogen and non-hydrogen atoms) was refined to a standard agreement factor ( $R$  value) of 0.026 (8).

Tris crystallizes in a layered structure with strong hydrogen bonds within each layer and weak hydrogen bonds between the layers. The important features of this structure are shown in Figs. 1 and 2 and Tables 1 through 3. All three hydroxyl hydrogen atoms are strongly intermolecularly hydrogen bonded to O(2), O(3), and N atoms within each layer,

whereas one of the amine hydrogen atoms is weakly hydrogen-bonded to an O(1) atom on a molecule in an adjacent layer. The role of O(1) as an acceptor of this weak hydrogen bond (from the amine hydrogen) is clearly evident from the highly anisotropic thermal ellipsoid of O(1) and consequently from the artificially short O(1)–H(1) bond length (for which, of course, no thermal riding correction has been applied).

Pentaerythritol, tris, and other substituted pentaerythritol compounds have similar high-temperature phases (5) in which the centers of the orientationally disordered molecules are located on the lattice points of face-centered cubic (fcc) unit cells. As the temperature is lowered, these crystals undergo solid-solid phase transitions to ordered systems of lower crystallographic symmetry. Detailed studies of the structures of the high- and low-temperature phases of a number of structurally similar molecules are often sufficient to allow one to relate the changes in positional parameters that accompany the phase transitions to the mechanisms of these phase transitions (9).

Although this aspect of the present study is still in the preliminary stages, it

is evident that the orthorhombic tris unit cell is formed by a contraction of the high-temperature fcc unit cell. A different situation is observed in pentaerythritol (6), where the fcc cell forms a centered tetragonal cell in which the  $a$  and  $b$  axes equal one-half of the fcc face diagonals and the  $c$  axis remains parallel and nearly equal to the third edge of the fcc unit cell.

However, even though the unit cells and crystal structures of the ordered phases of these two compounds are different, the gross features of the molecular packing in these ordered phases are similar. One can consider the center-to-center distances of nearest-neighbor molecules as indicators of the broad structural features that are of interest in these pseudospherical molecules, since these remain essentially the same in all phases.

Thus, in the high-temperature fcc phases of both compounds the center-to-center distances are close to 6.3 Å; in tetragonal pentaerythritol they are all 6.1 Å, whereas in orthorhombic tris they are 5.31, 5.87, and 5.94 Å. These figures indicate that during the phase transition in tris there are small contractions in two directions accompanied by a contraction of nearly 1 Å in the third direction (parallel to the orthorhombic  $b$  axis).

REUBEN RUDMAN

DONNA EILERMAN

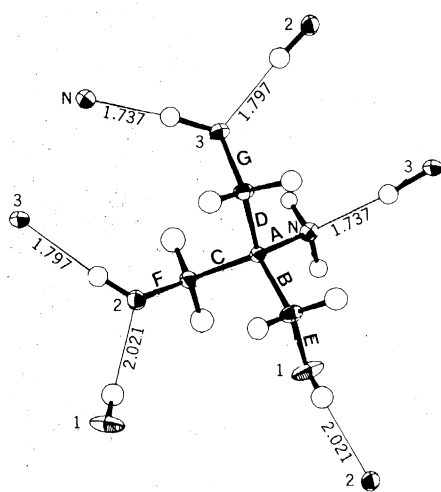
Chemistry Department, Adelphi University, Garden City, New York 11530

SAM J. LA PLACA

T. J. Watson Research Laboratory

International Business Machines Corporation,

Yorktown Heights, New York 10598



the unit cell and showing the intermolecular hydrogen bonding within each layer of molecules. Atoms N, O(1), O(2), and O(3) are designated by  $N$ , 1, 2, and 3, respectively. The hydrogen-bonded distances are given in angstroms, and the values of the intramolecular distances (identified by the letters A through G) are given in Table 1. Fig. 2 (right). Diagram of crystalline tris looking down the  $c$  axis of the unit cell. The layers are approximately perpendicular to the  $a$  axis. The hydrogen bonds within each layer are shown by the light lines between molecules; hydrogen bonds between the layers are not indicated.

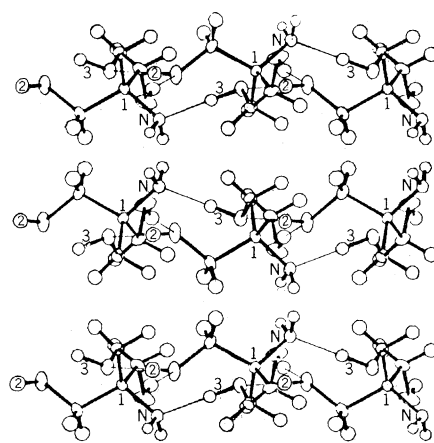


Fig. 1 (left). Diagram of a single molecule of tris looking approximately down the  $a$  axis of the unit cell.

Fig. 2 (right). Diagram of crystalline tris looking down the  $c$  axis of the unit cell. The layers are approximately perpendicular to the  $a$  axis. The hydrogen bonds within each layer are shown by the light lines between molecules; hydrogen bonds between the layers are not indicated.

#### References and Notes

- R. G. Bates and R. A. Robinson, *Anal. Chem.* **45**, 420 (1973).
- R. W. Ramette, C. H. Culberson, R. G. Bates, *ibid.* **49**, 867 (1977).
- W. A. Wilson, M. T. Clark, T. C. Pellmar, *Science* **196**, 440 (1977).
- L. D. Hansen and E. A. Lewis, *J. Chem. Thermodyn.* **3**, 35 (1971); R. Rychly and V. Pekarek, *ibid.* **9**, 391 (1977).
- N. Doshi, M. Furman, R. Rudman, *Acta Crystallogr. Sect. B* **29**, 143 (1973).
- I. Nitta and T. Watanabe, *Bull. Chem. Soc. Jpn.* **13**, 28 (1938).
- G. Némethy and H. A. Scheraga, *J. Phys. Chem.* **81**, 928 (1977).
- Experimental details are as follows. We collected data from an approximately spherical crystal 0.28 mm in diameter ( $\mu R = 0.13$ , where  $R$  is the radius of the crystal and  $\mu$  is its coefficient of linear absorption, no absorption corrections applied) on a CAD-4 diffractometer to ( $\sin \theta / \lambda_{\max} = 0.62$ , where  $\theta$  is the diffraction angle and  $\lambda$  is the wavelength, using nickel-filtered  $\text{CuK}\alpha$  radiation). The 1371 reflections that were measured yielded 672 unique reflections (of which only eight were unobserved); all the data were used in refinement. We solved the structure with the MULTAN program, using 100  $E$  factors ( $E$  is the normalized structure factor) greater than 1.32. We observed all nonhydrogen atoms on the  $E$  map obtained by using the phases corresponding to the highest combined figure-of-merit. Hydrogen atom positions were calculated for the six methylene hydrogen atoms; the remain-

ing five hydrogen atoms were subsequently located on difference Fourier maps after two iterations. The maximum peak height on a complete difference Fourier map was 0.18 electron per cubic angstrom. Full-matrix least-squares refinement of 117 parameters included an isotropic extinction parameter, anisotropic thermal parameters for the nonhydrogen atoms, and isotropic thermal parameters for the hydrogen atoms. The y coordinate of the central carbon atom was held constant. The atomic scattering factors found in the *International Tables for Crystallography* (Kynoch, Birmingham, En-

gland, 1974), vol. 4, were used; those for C, N, and O are found on p. 73, and the H scattering factors are listed on p. 102. Refinement continued until the parameter shifts were less than  $2 \times 10^{-7}$  with a goodness-of-fit of 0.902. The final agreement factors were  $R = 0.026$  and  $R_w$  (weighted  $R$  value) = 0.038.

9. R. Rudman, *J. Chem. Phys.* **66**, 3139 (1977).  
10. The research at Adelphi University was supported under NSF grants CHE 75-13935 and DMR 76-20639.

20 October 1977; revised 24 January 1978

## Chemistry of Oceanic Particulate Matter and Sediments: Implications for Bottom Sediment Resuspension

**Abstract.** *Analyses of suspended particulate matter from the eastern equatorial Pacific Ocean have defined a 400-meter-thick benthic nepheloid layer enriched in aluminum, silicon, iron, and manganese relative to the overlying waters. Chemical mass-balance calculations suggest that the concentration increases in the benthic nepheloid layer are due to resuspension from the fraction of the local bottom sediments in the size range  $\leq 1$  micrometer.*

A benthic nepheloid layer (BNL) is nearly ubiquitous in the deep sea (1), but the processes that generate and maintain this feature are poorly understood. Light scattering profiles and current meter measurements in high-energy environments along the continental margins (2) and in abyssal topographic gaps such as the Vema Channel (3) suggest that the thickness and intensity of the BNL are a function of current speed, bathymetry, or both; this is strong circumstantial evidence that bottom sediment resuspension is an important factor in maintaining the BNL. The efficiency of resuspension in the lower-energy environments of the ocean basins, however, is inherently more suspect. Compositional factors of oceanic particulate matter can be sensitive indicators of benthic processes (4), although sampling and analytic difficulties have severely limited this approach in the deep sea. We report here on changes in the particulate chemistry within the BNL relative to both the overlying clearer water and the underlying bottom sediments. Our evidence suggests that significant resuspension of the fine fraction ( $\leq 1 \mu\text{m}$ ) of deep-sea sediments can occur under the influence of even moderate benthic currents (mean speed  $< 8$  cm/sec).

Samples of suspended particulate matter (SPM) were collected in 30-liter polyvinyl chloride sampling bottles from depths below 450 m at three stations (A at  $8^{\circ}27'N$ ,  $150^{\circ}47'W$ ; B at  $11^{\circ}42'N$ ,  $138^{\circ}24'W$ ; and C at  $15^{\circ}00'N$ ,  $126^{\circ}00'W$ ) in the eastern equatorial Pacific manganese nodule province. The particulate matter was collected on Nuclepore membrane filters (pore size,  $0.4 \mu\text{m}$ ) by closed-system filtration and analyzed for Al, Si, Mn, and Fe by secondary emis-

sion thin-film x-ray fluorescence (5). A sample of the surficial bottom sediment was collected at each station by a box corer.

The regional thickness of the BNL, on the basis of sharply increased Al percentages in the SPM, is approximately 400 m (Fig. 1). Total SPM concentrations within this layer are 10 to 40 percent above the midwater average of  $\sim 9 \mu\text{g/liter}$ . Scatter diagrams of the Si, Mn, and Fe concentrations versus the Al concentration (Fig. 2) define the chemical characteristics of the BNL and describe some important interelement relationships.

Particulate Si (Fig. 2a) is mostly biogenic ( $>$  about 75 percent) above the BNL, its average concentration is 12.3 percent by weight, and it is poorly correlated with Al ( $r = .25$ ). Within the BNL, Si is highly correlated with Al ( $r = .89$ ), although the average Si/Al ratio (4.3) is higher than the average for eastern central Pacific sediments ( $\sim 3.0$ ) (6), which

suggests the presence of some residual biogenic Si debris, particularly since these stations are positioned above the equatorial band of siliceous ooze (6). The pattern for Fe and Mn is more complex. The percentages of both elements increase significantly within the BNL relative to the overlying waters (Fig. 2, b and c), but their variation within the BNL is only moderately correlated with that of Al, signifying that at least one other phase besides the aluminosilicates influences the distribution of Fe and Mn.

The BNL in this region may be due to either or both of two effects: accumulation of sinking particles from water layers at the surface and middle depths, or resuspension of some fraction of the bottom sediments, either locally or up-current from the study area. The accumulation hypothesis requires an extensive change in the particulate chemistry as the sinking suspended matter reaches the BNL. An increase in the weight percentages of Al, Si, Fe, and Mn would result if other fractions low in these elements—such as  $\text{CaCO}_3$  and particulate organic matter—were preferentially lost from the BNL, but the observed increases in absolute SPM concentration and the highly variable enrichment (0.9 to 5.1) of these elements within the BNL argue against this mechanism. Similarly, a complicated differential settling scheme might be devised for each station to produce the observed enrichment, but would require unrealistic settling velocity differences to account for the two- to fivefold increases in Al within the BNL.

Alternatively, resuspension can alter the BNL chemistry by selectively injecting a chemically distinct fraction of the bottom sediment. Samples of the surficial bottom sediment from each station were therefore size-fractionated by settling in distilled water, and portions of the fine ( $\leq 1 \mu\text{m}$ ) fraction (44 to 76 per-

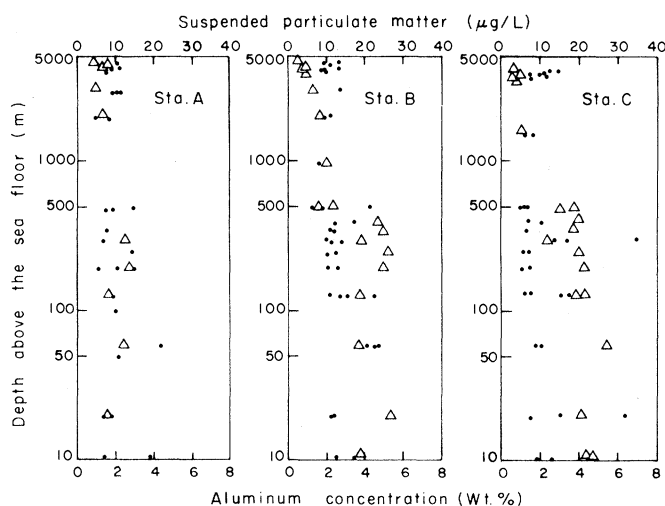


Fig. 1. Suspended particulate matter concentration (●) and percentage Al by weight (Δ) in the water column at three stations in the eastern equatorial Pacific. Note that the depth scale is logarithmic.